Original Research   *Neuroradiology/Head and Neck Imaging*

Magnetic resonance imaging in COVID-19-associated acute invasive fungal rhinosinusitis – Diagnosis and beyond

Gayatri Senapathy[1], Tharani Putta[1] (iD), Srinivas Kishore Sistla[2]

Departments of [1]Radiology and [2]ENT, Asian Institute of Gastroenterology Hospitals, Hyderabad, Telangana, India.

*Corresponding author:
Gayatri Senapathy,
Department of Radiology,
Asian Institute of
Gastroenterology Hospitals,
Hyderabad, Telangana, India.

sgayatri0311@gmail.com

ABSTRACT

Objectives: The aim of the study was to evaluate the magnetic resonance imaging (MRI) features of acute invasive fungal rhinosinusitis (AIFRS) at presentation and on follow-up imaging when patients receive treatment with systemic antifungal therapy and surgical debridement.

Material and Methods: This is a retrospective analysis of imaging data from a cohort of patients diagnosed with AIFRS during the second wave of COVID-19 in single tertiary referral hospital in South India between March 2021 and May 2021 ($n = 68$). Final diagnosis was made using a composite reference standard which included a combination of MRI findings, clinical presentation, nasal endoscopy and intraoperative findings, and laboratory proof of invasive fungal infection. Analysis included 62 patients with "Definite AIFRS" findings on MRI and another six patients with "Possible AIFRS" findings on MRI and laboratory proof of invasive fungal infection. Follow-up imaging was available in 41 patients.

Results: The most frequent MRI finding was T2 hypointensity in the sinonasal mucosa (94%) followed by mucosal necrosis/loss of contrast-enhancement (92.6%). Extrasinosal inflammation with or without necrosis in the pre-antral fat, retroantral fat, pterygopalatine fossa, and masticator space was seen in 91.1% of the cases. Extrasinosal spread was identified on MRI even when the computed tomography (CT) showed intact bone with normal extrasinosal density. Orbital involvement (72%) was in the form of contiguous spread from either the ethmoid or maxillary sinuses; the most frequent presentation being orbital cellulitis and necrosis, with some cases showing extension to the orbital apex (41%) and inflammation of the optic nerve (32%). A total of 22 patients showed involvement of the cavernous sinuses out of which 10 had sinus thrombosis and five patients had cavernous internal carotid artery involvement. Intracranial extension was seen both in the form of contiguous spread to the pachymeninges over the frontal and temporal lobes (25%) and intra-axial involvement in the form of cerebritis, abscesses, and infarcts (8.8%). Areas of blooming on SWI were noted within the areas of cerebritis and infarcts. Perineural spread of inflammation was seen along the mandibular nerves across foramen ovale in five patients and from the cisternal segment of trigeminal nerve to the root exit zone in pons in three patients. During follow-up, patients with disease progression showed involvement of the bones of skull base, osteomyelitis of the palate, alveolar process of maxilla, and zygoma. Persistent hyperenhancement in the post-operative bed after surgical debridement and resection was noted even in patients with stable disease.

Conclusion: Contrast-enhanced MRI must be performed in all patients with suspected AIFRS as non-contrast MRI fails to demonstrate tissue necrosis and CT fails to demonstrate extrasinosal disease across intact bony walls. Orbital apex, pterygopalatine fossa, and the cavernous sinuses form important pathways for disease spread to the skull base and intracranial compartment. While cerebritis, intracranial abscesses, and infarcts can be seen early in the disease due to the angioinvasive nature, perineural spread and skull base infiltration are seen 3–4 weeks after disease onset. Exaggerated soft-tissue enhancement in the post-operative bed after debridement can be a normal finding and must not be interpreted as disease progression.

Keywords: Mucormycosis, Fungal sinusitis, Rhinosinusitis, COVID-19, MRI

INTRODUCTION

The baseline incidence of acute invasive fungal rhinosinusitis (AIFRS) is low and often limited to patients with uncontrolled diabetes and immunocompromised state.[1] The second wave of the COVID-19 pandemic in India, between March and July 2021, saw an unprecedented surge in acute invasive rhino-orbital fungal sinusitis, which prompted the government of India to declare COVID-19-associated mucormycosis (CAM) a notifiable disease under Epidemic Diseases Act in May 2021.[2]

This unfortunate situation presented us with the opportunity to evaluate the magnetic resonance imaging (MRI) features of AIFRS at presentation and on follow-up imaging when patients received treatment with systemic antifungal therapy and surgical debridement. AIFRS is characterized by rapid onset of illness (<4 weeks) with vascular invasion and thrombosis, resulting in infarction and tissue necrosis with a very aggressive clinical course.[3] The early angioinvasive nature of the disease, which accounts for the rapid spread across intact bony walls, is often not demonstrated on computed tomography (CT) as bone destruction is a late finding.[3-5] Contrast-enhanced MRI (CE-MRI) in patients with a high index of clinical suspicion helps detect the early and specific signs of AIFRS, such as mucosal necrosis and perisinosal fat stranding before orbital and intracranial spread, thereby prompting early initiation of treatment.[3-8]

MATERIAL AND METHODS

This is a retrospective analysis of imaging data from a cohort of patients diagnosed with AIFRS in a single tertiary referral hospital as part of CAM. A total number of 68 patients were diagnosed with AIFRS between March 2021 and May 2021 in our center with inhouse MRI.

A composite reference standard was used to arrive at a diagnosis of AIFRS, which included in the study:
1. Definitive AIFRS on imaging plus one or more of the following:
    *   Clinical presentation highly suggestive of AIFRS
    *   Classic findings of invasive fungal rhinosinusitis on diagnostic nasal endoscopy
    *   Intraoperative appearance of invasive fungal infection and
    *   Laboratory proof of invasive fungal infection.
2. Possible AIFRS on imaging plus laboratory proof of invasive fungal infection with or without one of the following:
    *   Clinical presentation highly suggestive of AIFRS
    *   Classic findings of invasive fungal rhinosinusitis on diagnostic nasal endoscopy and
    *   Intraoperative appearance of invasive fungal infection.

Table 1: Magnetic resonance sequences.

DWI Whole Brain Axial, b-1000, NEX-1, ST 5 mm
Whole Brain FLAIR, NEX-1, ST 5 mm
SWIp–FAST Axial, ST 2 mm
Whole brain axial T1W, ST 5 mm
Coronal and axial small FOV T2W_TSE
for PNS and Orbits, ST 3.5 mm
Coronal and axial small FOV STIR_long
TE for PNS and Orbits, ST 3.6 mm
Axial small FOV T1_TSE for PNS and Orbits, ST 3.9 mm
Oblique sagittal T1W both orbits, ST 3 mm
Small FOV axial 3D_T1W_mDIXON for
PNS and Orbits, ST 2 mm
MR angiogram 3D TOF, ST 1. 4 m
Post-contrast axial T1_3D_TFE_FS, ST 1.2 mm
Post-contrast small FOV T1 SE Axial, ST 3.5 mm
Post-contrast small FOV T1 SE Coronal, Sagittal, ST 5 mm

DWI: Diffusion weighted imaging, NEX: Number of excitations, ST: Slice thickness, FLAIR: Fluid attenuated inversion recovery, SWI: Susceptibility weighted imaging, FOV: Field of view, PNS: Para nasal sinuses, STIR: Short tau inversion recovery, TSE: Turbo spin echo, TOF: Time of flight, TFE: Turbo field echo, SE: Spin echo, T1W: T1-weighted, T2W: T2-weighted

Table 2: Demographics, comorbidity, and imaging profile of AIFRS cases.

Features	*n*=68
Median age (range), in years	52 (24–79)
Gender	
Male	50
Female	18
Diabetes	
Known diabetic	35
Detected at presentation	24
Non diabetic	4
History not available	5
Concurrent or recent COVID-19 infection	68
History of steroid use for COVID-19 infection	
Present	28
Absent	5
History not available	35
Other immunocompromised conditions (post-transplant)	2
Magnetic resonance imaging	
Non-contrast	3
With contrast (CE-MRI)	65
Follow-up/Outcome at June 2022#	
Alive; Regression on imaging	14
Alive; Stable residual disease on imaging	4
Alive; Progression on imaging	19
Death	4
Lost to follow-up	27

#Last available follow-up imaging was assessed, ranging from June 2021 to June 2022. AIFRS: Acute invasive fungal rhinosinusitis, CE-MRI: Contrast-enhanced magnetic resonance imaging

Table 3: Causative fungal organism.

Pathogen	No. of patients
Mucorales	40
Aspergillus	9
Alternaria	1
Mucor+Aspergillus	2
Inconclusive[a]	3
No fungal growth/fungal elements detected[a]	8
No in-house laboratory tests performed	5
Total	68

[a]In these patients the diagnosis of AIFRS was based on "Definitive AIFRS" findings on CE-MRI together with a high index of clinical suspicion based on the clinical presentation and nasal endoscopy findings

Table 4: Frequency of paranasal sinus involvement on MRI (*n*=68).

Sinuses involved[a]	Number (%)
Maxillary	
Unilateral	22 (32.3)
Bilateral	45 (66.1)
Ethmoid	
Unilateral	17 (25.0)
Bilateral	47 (69.1)
Sphenoid	
Unilateral	17 (25.0)
Bilateral	40 (58.8)
Frontal	
Unilateral	21 (30.8)
Bilateral	30 (44.1)

[a]More than one paranasal sinus was involved in most patients.
MRI: Magnetic resonance imaging

Table 5: Summary of MRI findings in AIFRS patients (*n*=68).

Parameter	Number of patients (%)
T2 hypointense signal in the thickened sinonasal mucosa	64 (94.1)
Sinonasal necrosis	63 (92.6)
Turbinates	37 (60.6) (*n*=61)[a]
Nasal septum	11 (17.7) (*n*=62)[b]
Paranasal sinus wall	58 (89.2) (*n*=65)[c]
Extrasinosal soft-tissue involvement	
Pre and/or retroantral soft tissue	62 (91.1)
Pterygopalatine fossa	56 (82.3)
Masticator space	41 (60.3)
Orbital cellulitis	
Unilateral	41 (60.3)
Bilateral	8 (11.7)
Orbital apex involvement	
Unilateral	25 (36.7)
Bilateral	3 (4.4)
Optic nerve involvement	
Unilateral	20 (29.4)
Bilateral	2 (2.9)
Cavernous sinus involvement	
Unilateral	20 (29.4)
Bilateral	2 (2.9)
Sinuses inflamed (*n*=136)	14 (10.3)
Sinuses thrombosed (*n*=136)	10 (7.3)
Extra-axial intracranial involvement (Pachymeningeal thickening and enhancement)	17 (25.0)
Intra-axial intracranial involvement (cerebritis/abscess/infarct)	12 (17.6)
Major vascular involvement (thrombosis, vasculitis)	6 (8.8)

Although the total number of cases was 68. [a]Necrosis could not be assessed in four patients who had prior turbinectomy and in three patients who had non-contrast MRI, therefore *n*=61. [b]Necrosis could not be assessed in three patients who had prior nasal septum resection and in three patients who had non-contrast MRI, therefore *n*=62. [c]Necrosis could not be assessed in three patients who had non-contrast MRI, therefore *n*=65. MRI: Magnetic resonance imaging, AIFRS: Acute invasive fungal rhinosinusitis

All the patients had MRI of the orbits, paranasal sinuses (PNSs), and brain. Sixty-five out of the 68 had CE-MRI; three had non-contrast MRI in view of deranged renal function parameters.

Imaging follow-up was available between 1 and 13 months of disease onset in 41 out of the 68 patients.

MRI protocol

All the patients underwent MRI on Philips MR Systems Ingenia S, 1.5 Tesla, Release 5.7. MRI brain with additional dedicated sequences for the orbits and PNS were performed. The contrast used was MultiHance (gadobenate dimeglumine, 529 mg/mL) administered with a pressure injector at a dose of 10 mL IV at 2 mL/s flow rate, followed by 15 mL saline chase at 2 mL/s flow rate. In patients where intracranial major vessel involvement was suspected, 3D Time of flight magnetic resonance angiography of the intracranial vessels was additionally obtained.

Magnetic resonance sequences are listed in [Table 1].

All the cases were read independently by two radiologists (SG and TP), both having an experience of more than 10 years in cross sectional imaging, and the final interpretation was based on consensus.

The MR images were evaluated for the presence or absence of findings related to AIFRS:
- Inflammation/infiltration was defined as T2 and short tau inversion recovery (STIR) hyperintense signal in the soft tissues with or without enhancement
- Necrosis or devitalized tissue was documented when the thickened sinonasal mucosa or adjacent inflamed soft tissues showed areas of non-enhancement[9,10]
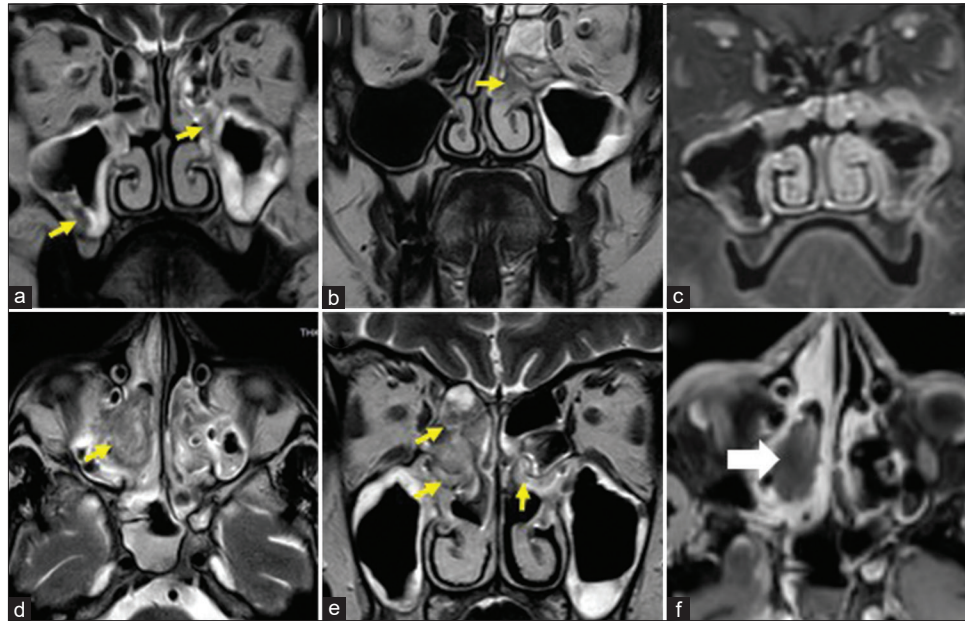
Figure 1: Early disease in two different patients, confined to the sinonasal cavity with no extrasinosal spread. Case1 (a-c) – A 62-year-old man: Coronal T2-weighted (T2W) magnetic resonance imaging (MRI) (a and b) and coronal post-contrast T1 fat saturation (T1-FS) MRI (c) demonstrate mucosal thickening with areas of T2 hypointense signal in bilateral maxillary and ethmoid sinuses (yellow arrows in a and b) with predominantly preserved enhancement (c). Case 2 (d-f) – A 30-year-old man: Axial T2W (d), coronal T2W (e) and axial post-contrast T1-FS MRI (f) demonstrate mucosal thickening with heterogeneous signal intensity over the bilateral middle turbinates and right ethmoid sinus (yellow arrows in d and e) with a large non-enhancing necrotic area (white block arrow).
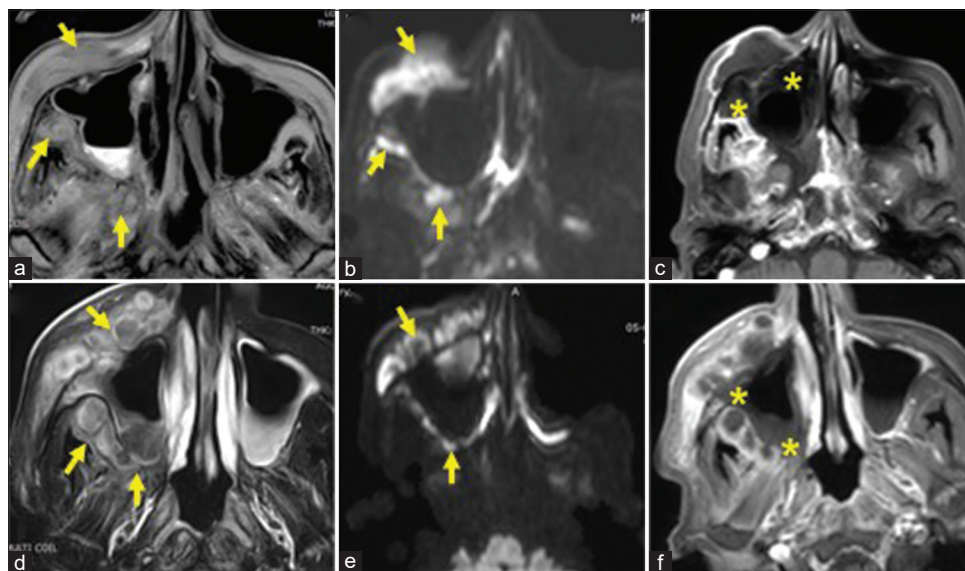

Figure 2: Extensive extrasinosal disease with necrosis in two different patients with acute invasive fungal rhinosinusitis. Case 1 (a-c) and Case 2 (d-f) with representative axial T2-weighted (a) T2 fat saturation (d), diffusion-weighted imaging (b and e) and post contrast T1 fat saturation magnetic resonance imaging (c and f) demonstrate extensive necrosis in the mucosa and bony walls of right maxillary sinus (yellow * in c and f), extrasinosal necrosis with abscess formation and diffusion restriction in the right pre-antral fat, retroantral fat, and pterygopalatine fossa (yellow arrows).
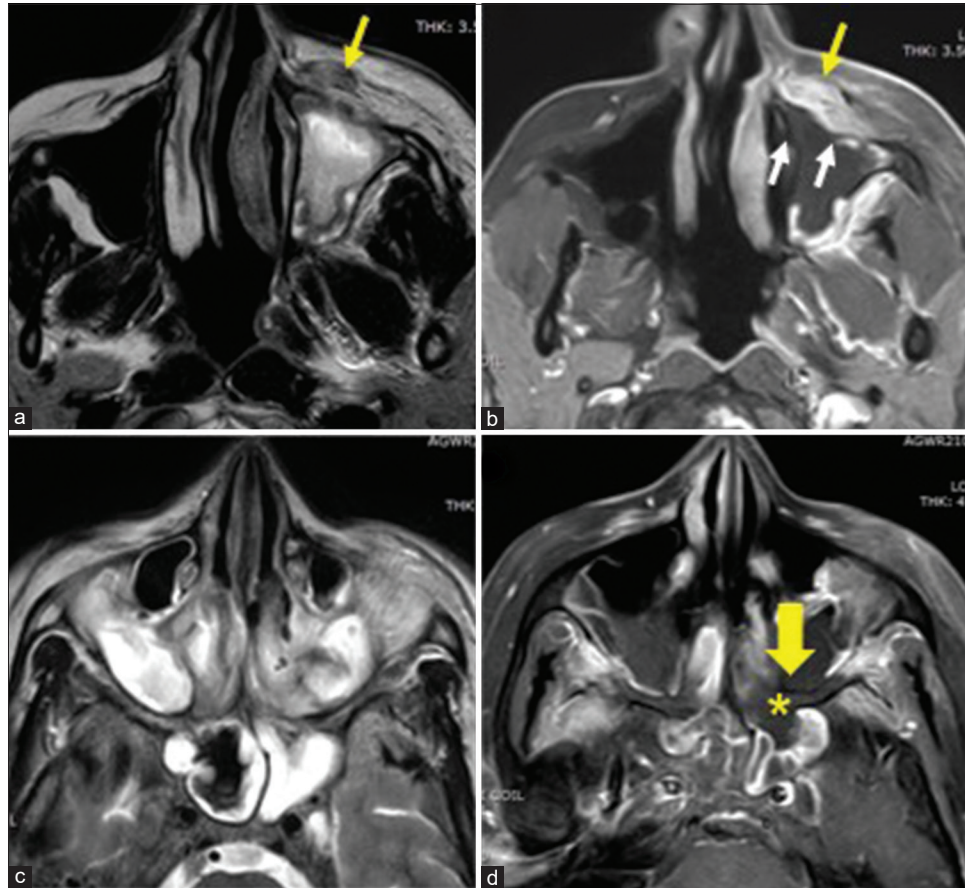
Figure 3: Extrasinosal extension of disease in two different patients. Case 1 (a and b) with representative axial T2-weighted (T2W) magnetic resonance imaging (MRI) (a) and axial post-contrast T1 fat saturation (T1-FS) MRI (b) showing left maxillary sinusitis with necrosis along its anterior and medial walls (white arrows in a and b) and extension of T2 hypointensity with abnormal enhancement of the left pre-antral fat (yellow arrow in a and b). Case 2 (c and d) with representative axial T2W MRI (c) and axial post-contrast T1-FS MRI (d) showing bilateral maxillary and sphenoid sinusitis (c) with devitalization of the posterior wall of left maxillary sinus (yellow block arrow in d) and extension of necrosis into the left retroantral fat (yellow *).

- PNS and nasal cavity: The nasal turbinates, nasal septum, and PNS were assessed for the presence of mucosal thickening, their T2 signal intensity, and necrosis.
- *Extrasinosal spread in the form of inflammation ± necrosis was documented in the following areas:*
  - Pre-antral fat, retroantral fat, pterygopalatine fossa, masticator space, temporal fossa, bony walls of the PNS, other bones including alveolus, palate, zygoma, and the skull base.
  - Orbit: cellulitis was documented when there was fat stranding in the orbital fat ± abscess, increased bulk with T2 hyperintense signal, and exaggerated enhancement in the extraocular muscles.
  - Optic nerve: Optic nerve thickening, T2/fluid attenuated inversion recovery (FLAIR)/diffusion-weighted imaging hyperintense signal, or exaggerated enhancement along the nerve were marked as inflammation. Marked diffusion restriction with or without necrosis was considered as optic nerve ischemia when associated with complete loss of vision. Orbital apices involvement was also separately documented.
- Cavernous sinuses: The presence of thickening, T2 hyperintensity, or enhancement along the lining dura was documented as involvement; thrombosis was defined as non-enhancement within the sinus cavity.
- Major intracranial vessels were assessed for the presence of vessel wall thickening and enhancement (documented as vasculitis) with or without thrombosis.
- Intracranial extra-axial involvement: Pachymeninges were assessed for both contiguous and non-contiguous thickening and enhancement.
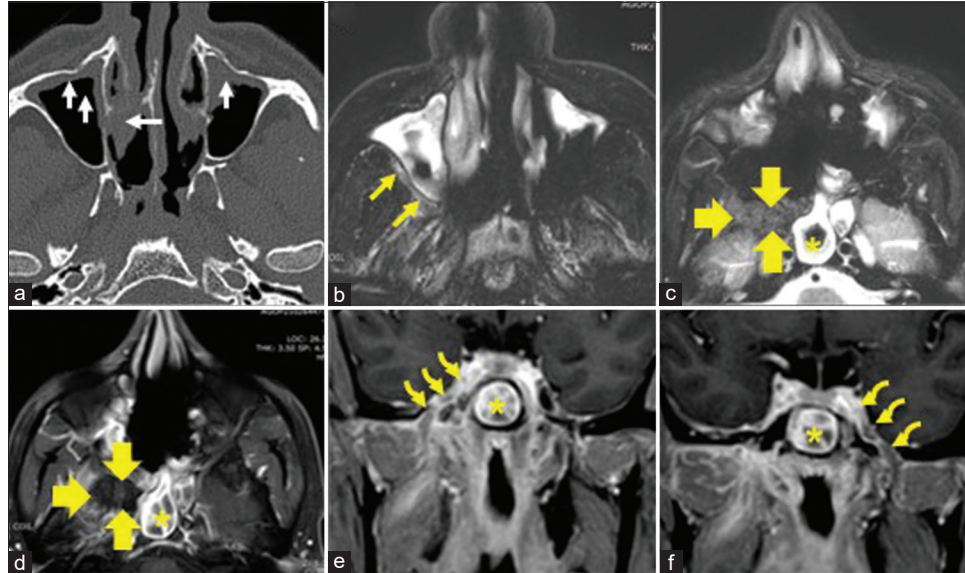
Figure 4: A 45-year-old man with diabetes and being treated for COVID-19 pneumonia. Axial computed tomography image (a) shows bilateral maxillary sinus and middle turbinate mucosal thickening (while arrows on a) with intact sinus wall and no apparent extrasinosal abnormality. Axial T2 fat saturation (T2-FS) magnetic resonance imaging (MRI) (b) done on the same day demonstrates unequivocal hyperintensity in the right retroantral fat (yellow arrows in b), indicating spread across intact bony sinus wall. He underwent resection of the right osteomeatal complex and turbinates with sinonasal debridement and was started on systemic antifungal therapy. Follow-up MRI done 3 weeks later (c-f) demonstrates disease progression with abnormal signal intensity on T2-FS axial image (c) and necrosis on post-contrast axial image (d) in the right pterygopalatine fossa and masticator space (yellow block arrows in c and d). There is new development of sphenoid sinusitis (yellow*) and perineural spread in the form of thickening and enhancement along bilateral mandibular nerves across the foramen ovale, into the cavernous sinuses (yellow curved arrows in e and f).

- Intracranial intra-axial involvement in the form of cerebritis, abscess, and infarcts was noted. The susceptibility weighted imaging (SWI) sequences were assessed for the presence of blooming.
- Perineural spread of disease: Abnormal T2/STIR hyperintense signal along the nerve ± enhancement.

The cases were categorized as "Possible AIFRS" or "Definite AIFRS" based on CE-MRI findings as follows:

Definitive AIFRS on CE-MRI = At least one of the two features was unequivocally present: mucosal necrosis and extrasinosal involvement. T2 hypointense signal in the mucosa of the sinus and/or turbinates may or may not be seen.

Possible AIFRS on CE-MRI = Definite T2 hypointense signal in the mucosa of the sinus and/or turbinates+ No or doubtful mucosal necrosis + No or doubtful extrasinosal involvement.

The radiologists were blinded to the clinical presentation, nasal endoscopy findings, intraoperative findings, and laboratory investigations at the time, the MRI scans were reviewed. Laboratory proof of causative organism (direct microscopy, histopathology with special stains, fungal culture, and molecular diagnostics), when available was documented by the other study participant.

In patients who had limited resection of the turbinates or sinuses before they presented to our center for MRI, the mucosa in the post-operative bed was assessed only for necrosis while the other areas were assessed for both inflammation and necrosis. Patients who underwent more extensive resection before presentation at our center were excluded from our study.

RESULTS

A total of 68 patients were included in our study, all of whom had either concurrent COVID-19 pneumonia or were diagnosed with COVID-19 infection within 45 days before presentation. [Table 2] summarizes the demographics, comorbidity, and imaging profile of the study patients and [Table 3] lists the causative fungal organism.

The most common clinical presentation was facial pain or numbness in the pre-maxillary region of a few days' duration, unilateral to begin with, and often associated with bloody

nasal discharge. Many of these progressed to have retro-orbital pain and proptosis in a few days.

Sixty-five out of the 68 patients underwent CE-MRI as per institutional protocol, while three underwent non-contrast MRI in view of deranged renal function parameters.

Imaging follow-up was available between 1 and 13 months from disease onset in 41 out of 68 patients.

Definitive AIFRS findings were found in 62/68 cases. The other six cases were categorized as "Possible AIFRS" based on MRI findings; all these cases had laboratory proof of invasive fungal infection.

PNS involvement on MRI

Most cases showed involvement of more than one sinus, with the most frequent combination being maxillary + ethmoid sinuses [Table 4]. The earliest and most frequent MRI finding was T2 hypointense signal in the thickened PNS mucosa (94%); the second most frequent finding was necrosis (92.6%) [Figure 1 and Table 5].

Extrasinosal involvement on MRI [Table 5]

The pre-antral and retroantral fat involvement was mostly in the form of fat stranding, followed by obliteration of the fat with inflammatory and/or necrotic tissue. Pre-antral abscess in the form of central necrotic collection with diffusion restriction and peripheral rim enhancement was seen in six out of 68 patients [Figure 2]. Retroantral fat involvement was often associated with extension into the pterygopalatine fossa [Figures 2-4]

Orbital cellulitis (72%) was seen more commonly in the extraconal and in some cases, also in the intraconal compartment. The medial and inferior recti were the most frequently involved extraocular muscles, in continuity with the adjacent PNS [Figures 5-7]. Orbital necrosis was seen in six patients [Figures 5 and 8].

Optic nerve involvement, when present, was always seen along with orbital cellulitis. Four patients had optic nerve ischemia out of which two were frank necrosis of the nerve seen contiguous with other orbital soft-tissue necrosis [Figures 5 and 8].

Conical deformity of the globe with anteroposterior elongation and posterior tenting, indicating the presence of tension orbit,[9] was seen in three patients [Figure 5]. Two patients had globe destruction with deformity [Figure 5].

All the patients with cavernous sinus involvement had either orbital apex, posterior ethmoid, or pterygopalatine fossa involvement [Figures 6, 8 and 9]. Five of these patients
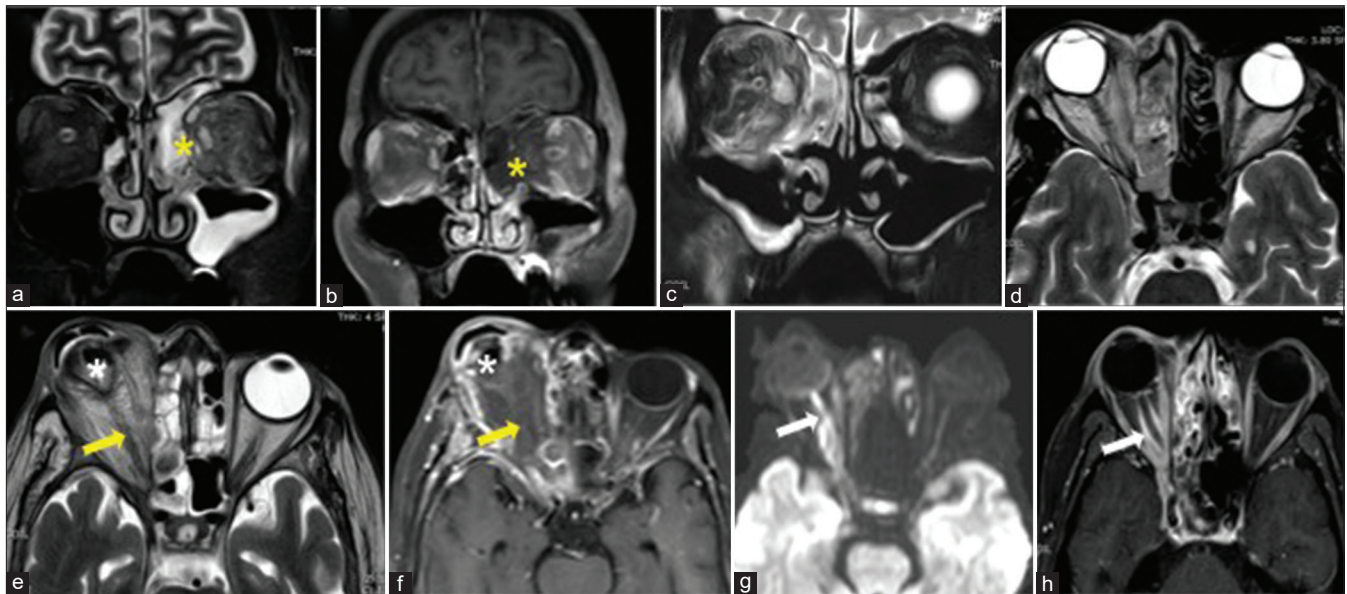

Figure 5: Demonstrating the spectrum of orbital involvement in four different acute invasive fungal rhinosinusitis cases. Case 1 (a and b) with coronal T2 fat saturation (T2-FS) and post-contrast T1 fat saturation (T1-FS) magnetic resonance (MR) images showing left maxillary and ethmoid sinusitis with contiguous extension of necrotic tissue from the left ethmoid sinus into the left orbit across the medial wall (yellow *). Case 2 (c and d) with coronal T2-FS and axial T2-weighted (T2W) MR images showing right ethmoid sinusitis, right orbital cellulitis (c), and proptosis with posterior tenting of the globe (d). Case 3 (e and f) with axial T2W and post-contrast T1-FS MR images showing extensive necrosis in the right orbit and optic nerve (yellow arrow in e and f) with globe destruction and deformity (white *). Case 4 (g and h) with axial diffusion-weighted imaging and post-contrast T1-FS MR images showing marked diffusion restriction of the right optic nerve (white arrow in g) with perineural enhancement (white arrow in h).
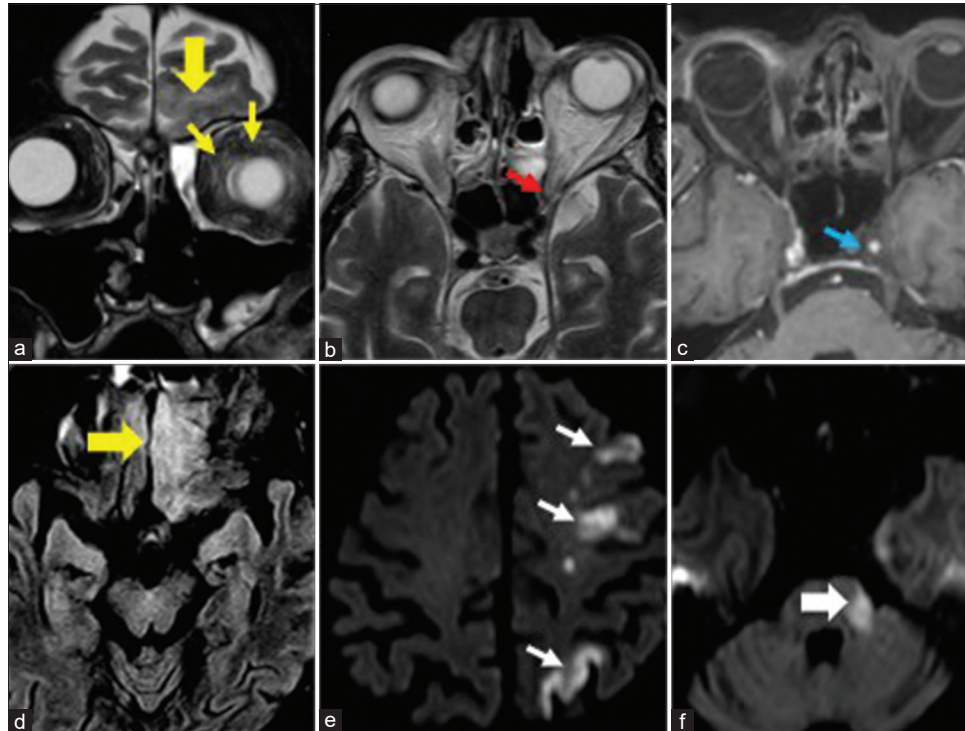
Figure 6: A 74-year-old man on treatment for COVID-19-related acute invasive fungal rhinosinusitis. Representative coronal T2 fat saturation (a), axial T2 (b), axial post-contrast T1 fat saturation (c) images through orbits and para nasal sinuses demonstrate left orbital cellulitis (yellow arrows in a) extending up to the orbital apex (red arrow in b) and left cavernous sinus causing thrombosis of the sinus and narrowing of left cavernous internal carotid artery (ICA) (blue arrow in c). Axial fluid attenuated inversion recovery image through brain (d) and image "a" show intracranial extension of inflammation across the orbital roof with cerebritis in the left frontal lobe (yellow block arrows in a and d). Representative axial diffusion-weighted imaging sequences (e and f) demonstrate infarcts in the left ICA territory (white arrows in e) and restricted diffusion in the pons at the root exit zone of the left trigeminal nerve (white block arrow in f).

showed wall thickening and enhancement of the cavernous internal carotid artery (ICA) [Figure 6]; out of which three had ICA thrombosis [Figure 8]. One of the patients with pre-clival extension of necrotic tissue had basilar artery thrombosis.

Involvement of the bones of skull base was seen in 30% of the patients [Figure 8].

Pachymeningeal thickening and enhancement were seen initially in contiguity with either the involved ethmoid sinuses across the cribriform plate, orbital roof, frontal bones or the pterygopalatine fossa, and later progressing to diffuse pachymeningeal enhancement in some of the cases [Figures 8 and 9].

A total of nine out of 68 patients developed cerebritis of which seven were contiguous with the involved pachymeninges and two were seen in distant parenchyma [Figures 6 and 9]. In all these cases, the involved brain parenchyma showed T2, FLAIR hyperintense signal ±

patchy enhancement; six of these cases also showed areas of blooming [Figure 9].

All the five patients with cavernous ICA involvement and the one patient with basilar artery involvement showed cerebral infarcts [Figure 9]. Two other patients with cavernous sinus involvement developed ICA thrombosis and infarcts on follow-up imaging.

Five patients had cerebral abscess, out of which one was at presentation to the hospital [Figure 8]. The other four had cerebritis at presentation which progressed to abscess on follow-up imaging, despite initiation of treatment [Figure 9].

Perineural spread of inflammation along the mandibular nerves traversing across the foramen ovale was seen in five patients [Figure 4]; one patient had retrograde spread from the left optic nerve to optic tract [Figure 8]. Three other patients had retrograde spread of inflammation along the trigeminal nerve in the cisternal segment
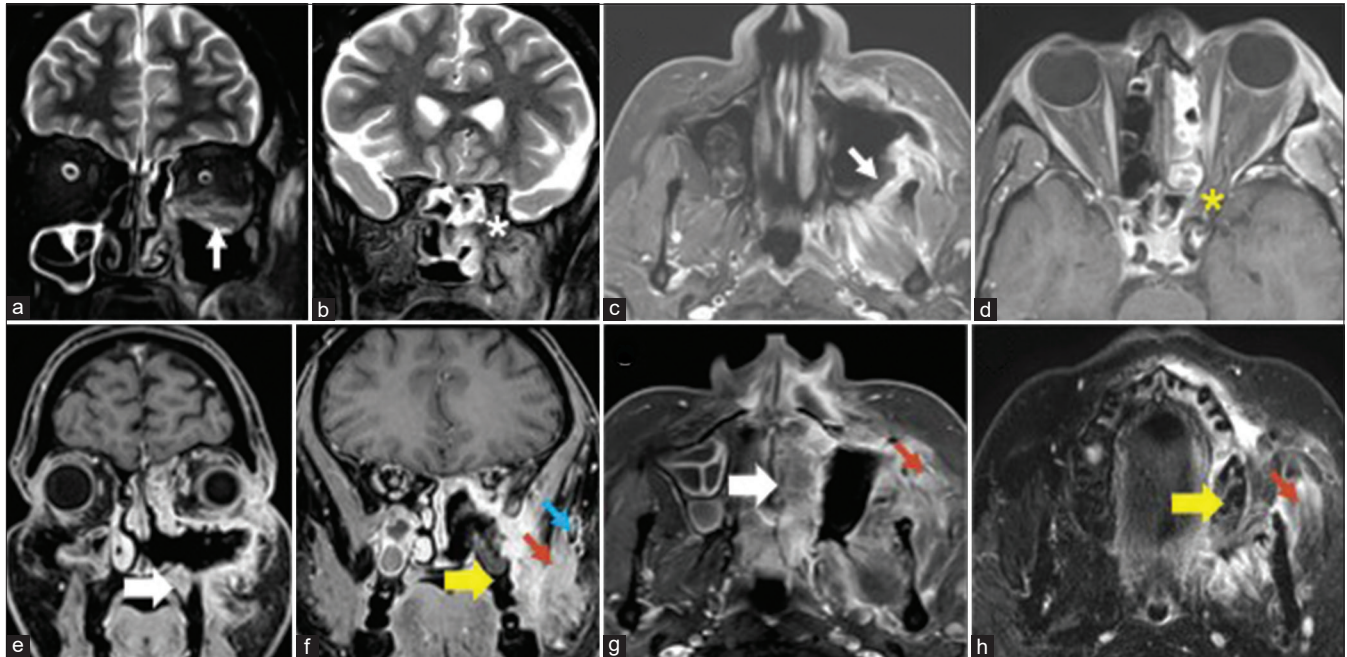
Figure 7: A 36-year-old man on treatment for COVID-19-related acute invasive fungal rhinosinusitis. Representative coronal T2 fat saturation (T2-FS) (a and b) and axial post-contrast T1 fat saturation (T1-FS) (c and d) images demonstrate left orbital and maxillary sinus involvement with necrosis in the bony walls of maxillary antrum (white arrows in a and c), extension of disease to the left orbital apex (yellow * in d) and left pterygopalatine fossa (white * in b). Endoscopic debridement and limited resection in the left maxilla and nasal cavity was performed. Follow-up imaging done after 6 weeks: Representative post-contrast T1-FS coronal and axial images (e-g) and axial T2-FS image (h) demonstrate involvement of the hard palate (white block arrows in e and g), alveolar process of left maxilla (yellow block arrows in f and h) and left zygoma (blue arrow in f) with extensive inflammation in the left masticator space and left temporal fossa (red arrows in f-h).

with infarcts or cerebritis in Pons at the root exit zone [Figure 6].

Few of the patients with extensive maxillary sinus and masticator space involvement also developed osteomyelitis of the palate ($n = 7$), the alveolar process of maxilla ($n = 8$), and zygoma ($n = 13$) during follow-up [Figure 7].

Some extent of surgical resection was seen in all the patients with follow-up studies, ranging from limited resection in the form of uncinectomy, turbinectomy, and ethmoidectomy to the more extensive forms such as orbital exenteration and maxillectomy. Most of these patients continued to show increased soft-tissue enhancement in the post-operative bed lasting for a few weeks after debridement [Figure 10]. Eight patients had follow-up imaging available between 8 and 13 months after disease onset and two of these patients succumbed due to disease progression with intracranial abscesses and infarcts. The remaining were clinically free from the disease but had come for reconstructive facial surgeries due to the deformities cause by resections and erosions during active disease. Varying degrees of osteonecrosis in the craniofacial skeleton were noted in these patients on CT done for planning the reconstructive surgeries [Figure 10].

DISCUSSION

Fungal rhinosinusitis is broadly divided into invasive and non-invasive and the invasive type is further classified into three subtypes: Acute invasive, chronic invasive, and chronic granulomatous invasive forms.[11-13] Invasive fungal sinusitis is defined by the presence of fungal hyphae within the mucosa, submucosa, bone, or blood vessels of the PNSs.[11] AIFRS occurs in immunocompromised patients, predominantly in those belonging to one of the following two categories: One group is patients with diabetic ketoacidosis or uncontrolled diabetes. The other is those with an immunocompromised state with neutropenia due to causes such as chemotherapy, bone marrow transplant, steroid therapy, or immunosuppressive therapy for organ transplant.[3,11-14]

Secondary infections have been documented in patients affected with COVID-19 infection.[15,16] While a majority of these have been bacterial and fungal pulmonary infections, the COVID-19 pandemic also saw an unprecedented incidence of AIFRS cases in epidemic proportions.[1,9,15-19]

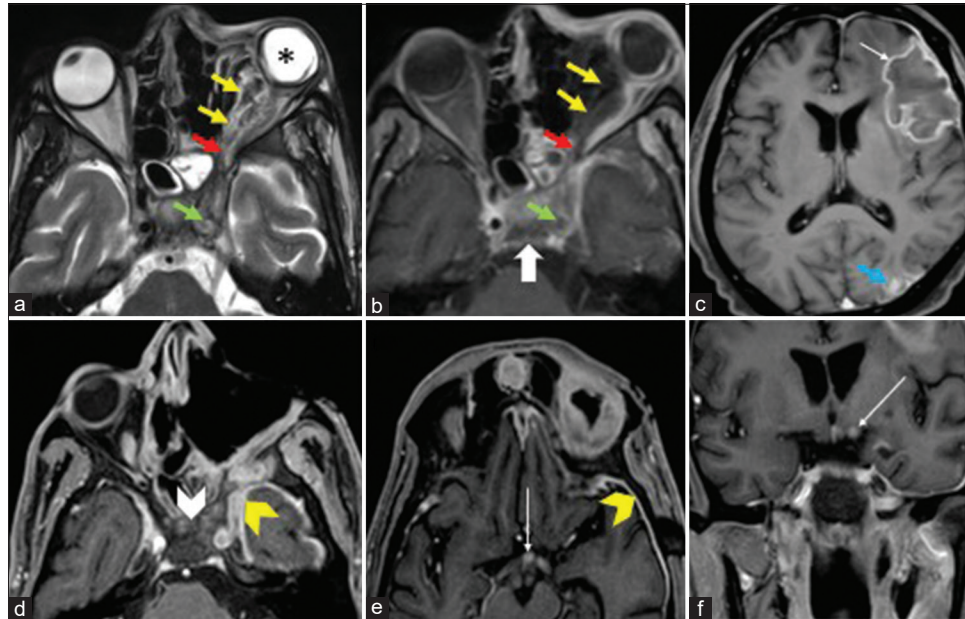Although there are no findings specific to COVID-19-related AIFRS as opposed to non COVID-19 related AIFRS, this

Figure 8: A 48-year-old man on treatment for COVID-19-related acute invasive fungal rhinosinusitis. Representative axial T2 fat saturation (a), axial T1 post-contrast (b and c) images demonstrating necrosis in the left orbit and left optic nerve (yellow arrows in a and b) extending to the orbital apex (red arrows in a and b) with globe deformity (* in a), left cavernous sinus and cavernous internal carotid artery (ICA) thrombosis (green arrows in a and b), osteomyelitis of the central skull base (white block arrow in b), abscess in the left frontal lobe (white arrow in c) and subacute infarct in the left parietal lobe (blue arrow in c). Follow-up scan after 7 weeks, post-left orbital exenteration: Representative axial T1 post-contrast (d and e) and coronal T1 post-contrast (f) images demonstrate increase in the extent of skull base osteomyelitis (white arrowhead in d) with pachymeningeal thickening and enhancement over left temporal lobe (yellow arrowheads in d and e). There is enhancement of the left optic chiasm and left optic tract (long white arrows in e and f) signifying intracranial extension of inflammation from the left optic nerve.

unfortunate situation presented us with the opportunity to document the temporal evolution of the CE-MRI findings in a large number of patients in a short time span. It also helped us identify the pattern of early and delayed craniofacial and intracranial complications in patients on treatment. The high index of clinical suspicion in this situation had also prompted early CE-MRI in many patients, which had also enabled us to document the very early and subtle changes on MR and we believe that this data can in future help in the early diagnosis of AIFRS in the vulnerable population much before orbital and intracranial spread.

The infection often arises in the nasal cavity, spreading to the PNS.[1,3,14] Spread to the orbits, pterygopalatine fossa, and intracranially is through direct invasion as well as by hematogenous spread in the form of vascular invasion and thrombosis, which accounts for the rapid and fulminant course of the disease.[3]

Plain CT scan of the PNSs initially shows non-specific hypodense mucosal thickening but, due to spread across intact bony walls, fails to demonstrate the early and specific signs of AIFRS such as mucosal necrosis and extrasinosal fat stranding [Figure 4].[3-8] Hence, all our patients referred for imaging with a high index of clinical suspicion of AIFRS based on history and clinical examination were subjected to CE-MRI rather than CT, in line with our institutional protocol.

T2 hypointense mucosal signal in the affected PNSs and turbinates is due to the T2 shortening effect of the fungal elements.[20] Although T1 hyperintensity ± T2 hypointensity of the sinus contents is also a feature of fungal sinusitis, it may also be seen with chronic and non-invasive forms of fungal sinusitis and when there are blood products within the sinus cavity.[6] Hence, this finding was deliberately not given weightage in our study.

Orbital involvement was seen as an extension from ethmoid sinusitis more often than maxillary sinusitis, possibly because of the porous lamina papyracea facilitating extrasinosal spread into the orbit. All the patients with optic nerve necrosis, extensive orbital necrosis, or globe destruction underwent orbital exenteration.
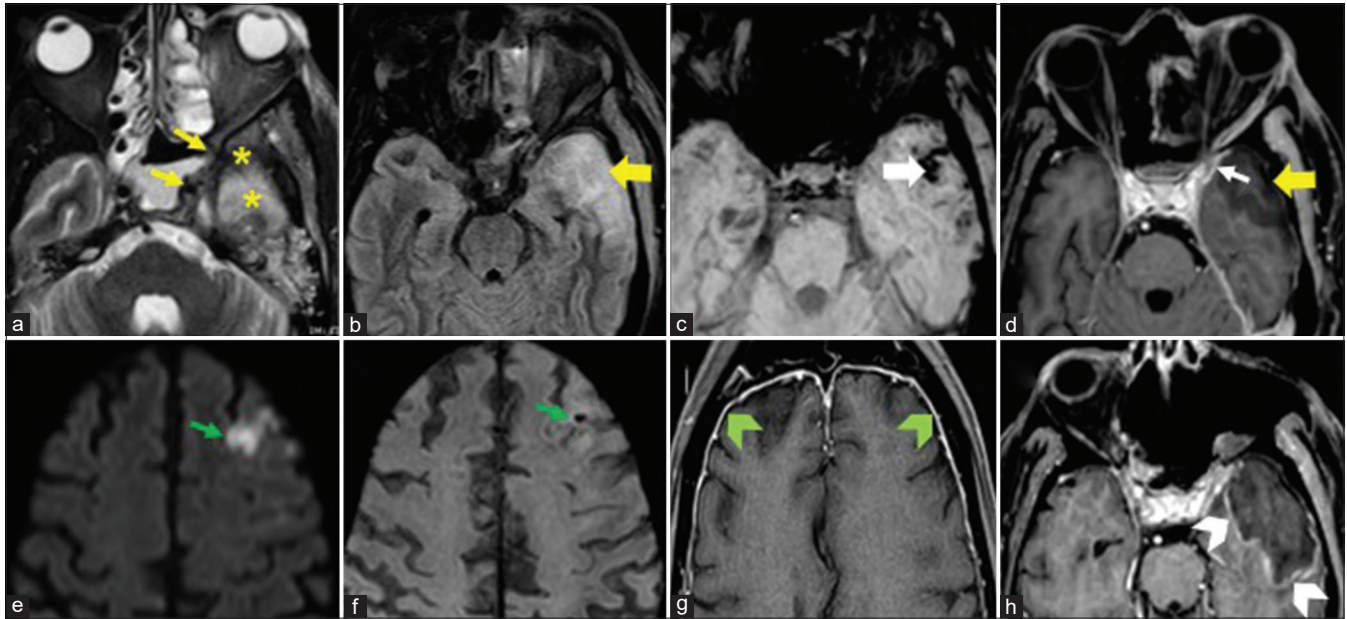
Figure 9: A 60-year-old man on treatment for COVID-19-related acute invasive fungal rhinosinusitis involving bilateral ethmoid sinuses and left orbital apex. Representative axial T2 fat saturation image (a) shows left orbital apex and cavernous sinus involvement (yellow arrows) with contiguous extension into the left retroantral fat and left temporal lobe (yellow*). Axial T2 Fluid attenuated inversion recovery (b), axial susceptibility-weighted imaging (SWI) (c) and axial post-contrast T1 fat saturation (T1-FS) (d) images show left temporal lobe cerebritis (yellow block arrows in b and d) with areas of blooming (white block arrow in c) and overlying dural thickening and enhancement (white arrow in d). The patient underwent sinonasal debridement and left orbital exenteration. Follow-up magnetic resonance imaging after 3 weeks: Axial diffusion-weighted imaging (e), axial SWI (f), and axial post-contrast T1-FS (g and h) images demonstrate interval development of the left frontal lobe infarct with blooming (green arrows in e and f), diffuse pachymeningeal thickening, and enhancement (green arrow heads in g) and evolution of the left temporal lobe cerebritis into an abscess with peripheral enhancement (white arrowhead in h).

Extension of the disease into the pterygopalatine fossa is by direct invasion from the maxillary sinus and through the inferior orbital fissure from the orbit, forming a pathway for further spread to masticator space, temporal fossa, and the cavernous sinuses, as seen in our study.[20] Some of these cases demonstrated frank necrosis in the form of sheet like non enhancing devitalized tissue, sometimes extending to the bones of the skull base and the adjacent pachymeninges. Apart from the bony walls of the sinus cavities, involvement of the other facial bones such as the hard palate, alveolar process of the maxilla, and zygoma was seen beyond 3–4 weeks of onset.

Meningitis and cerebral abscess are the most commonly described central nervous system (CNS) manifestations of invasive fungal infections.[21] Vascular complications such as vasculitis, mycotic aneurysm formation, cerebral hemorrhage, and ischemic infarction are the distant complications resulting from the hematogenous spread of fungal CNS infections due to their angioinvasive features.[21] In our study, cerebral infarcts/cerebritis were often seen at non-contiguous distant sites and showed blooming. Due to direct angioinvasive nature, the infarcts can harbor fungal elements. This, along with vasculitis, may explain blooming

on SWI sequences.[20] The ophthalmic and ethmoid arteries are the common vascular channels for intracranial spread, apart from the ICA when the cavernous sinus is involved.[20] A few of these infarcts/fungal cerebritis lesions progressed to abscess formation on follow-up imaging despite treatment.

Perineural spread of fungus through direct infiltration from the cavernous sinus to the brainstem has been described in literature.[22,23] This was seen as trigeminal nerve involvement in the cisternal segment and its root exit zone in Pons in our study in the form of T2/FLAIR hyperintensity and restricted diffusion. Involvement of the branches of trigeminal nerve in foramen ovale and foramen spinosum was a more common finding; one patient had retrograde spread along the left optic nerve to the optic tract; these were mostly observed after 3–4 weeks of disease onset on follow-up imaging in patients with disease progression.

On follow-up, most of the patients continued to show increased soft-tissue enhancement in the post-operative bed for a few weeks after debridement, even when there was unequivocal clinical improvement. We therefore believe that this finding in isolation cannot be considered
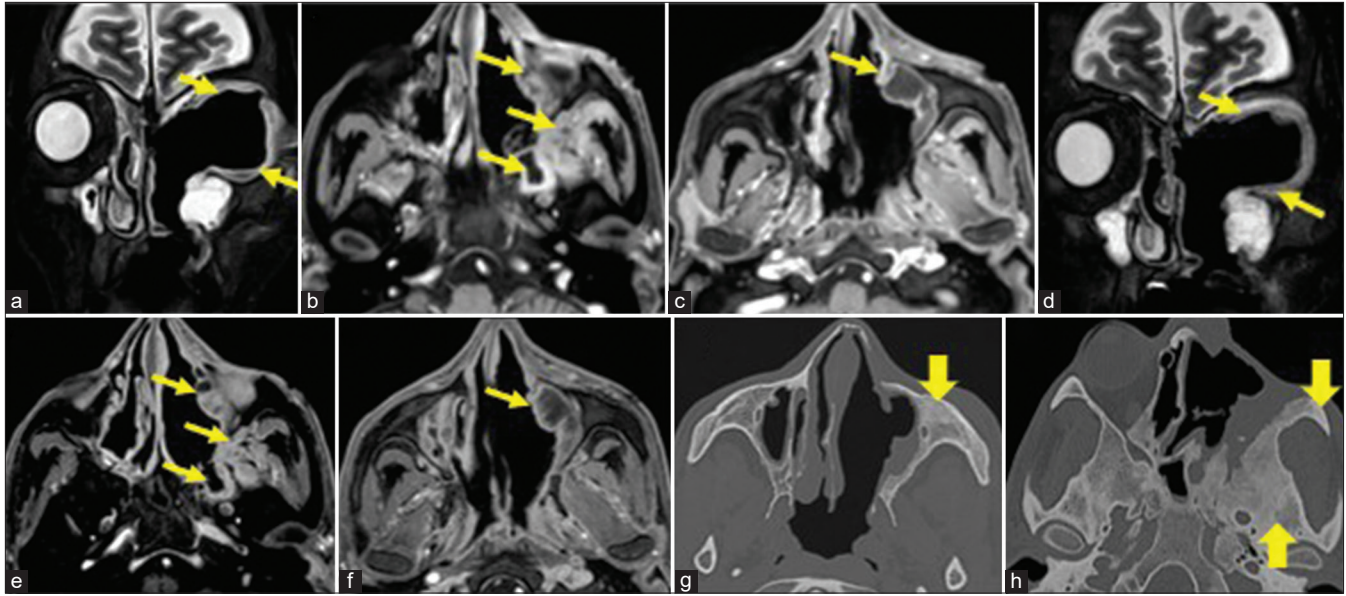
Figure 10: A 45-year-old man who was on treatment for extensive COVID-19-related acute invasive fungal rhinosinusitis for 3 months, had undergone bilateral sinonasal debridement, left maxillectomy and left orbital exenteration. Representative coronal T2 fat saturation (T2-FS) (a), axial post-contrast T1 fat saturation (b and c) images from contrast-enhanced magnetic resonance imaging (CEMRI) performed a week after orbital exenteration demonstrate enhancing soft tissue/mucosal thickening lining the post-operative bed (yellow arrows in a-c); no residual necrotic areas were seen. Follow-up CEMRI done 4 weeks later with representative images at the same levels (d-f) show persistent mild mucosal thickening and enhancement (yellow arrows in d-f) as in the previous MRI with no new areas of inflammation and no interval development of necrosis. The patient was on treatment with regular clinical monitoring and returned after 9 months for reconstructive facial surgery. Computed tomography of the para nasal sinuses done at this time (g and h) demonstrates changes of chronic osteomyelitis in the left maxilla, zygoma, and sphenoid bone (yellow block arrows).

as persistent disease. On follow-up imaging, presence of active or progressive disease may be identified when there is inflammation or necrosis at a new site.

CONCLUSION

CE-MRI must be performed in all cases with suspected acute angioinvasive fungal sinusitis as CT fails to demonstrate early extra sinosal disease spread across intact bony walls and non-contrast study fails to demonstrate tissue necrosis.

Orbital apex, pterygopalatine fossa, and the cavernous sinuses form important pathways for disease spread to the skull base and intracranial compartment.

While development of intracranial abscesses, infarcts, and cerebritis can be seen early in the disease due to angioinvasive nature, development of perineural spread and skull base infiltrations are seen 3–4 weeks after disease onset.

Exaggerated soft-tissue enhancement in the post-operative bed lasting a few weeks after debridement can be a normal finding and must not be interpreted as disease progression unless there is interval development of necrosis or inflammation at a new site.

Declaration of patient consent

Patient's consent not required as patient's identity is not disclosed or compromised.

Financial support and sponsorship

Nil.

Conflicts of interest

There are no conflicts of interest.

REFERENCES

1. Ismaiel WF, Abdelazim MH, Eldsoky I, Ibrahim AA, Alsobky ME, Zafan E, *et al.* The impact of COVID-19 outbreak on the incidence of acute invasive fungal rhinosinusitis. Am J Otolaryngol 2021;42:103080.
2. Sanghvi D, Kale H. Imaging of COVID-19-associated craniofacial mucormycosis: A black and white review of the "black fungus". Clin Radiol 2021;76:812-9.
3. Mossa-Basha M, Ilica AT, Maluf F, Karakoc O, Izbudak I, Aygun N. The many faces of fungal disease of the paranasal sinuses: CT and MRI findings. Diagn Interv Radiol 2013;19:195-200.
4. Khattar VS, Hathiram BT, Khattar VS, Hathiram BT. Radiologic

appearances in fungal rhinosinusitis. Otorhinolaryngol Clin Int J 2009;1:15-23.

5. DelGaudio JM, Swain RE Jr., Kingdom TT, Muller S, Hudgins PA. Computed tomographic findings in patients with invasive fungal sinusitis. Arch Otolaryngol Head Neck Surg 2003;129:236-40.

6. Ni Mhurchu E, Ospina J, Janjua AS, Shewchuk JR, Vertinsky AT. Fungal rhinosinusitis: A radiological review with intraoperative correlation. Can Assoc Radiol J 2017;68:178-86.

7. DeShazo RD, Chapin K, Swain RE. Fungal sinusitis. N Engl J Med 1997;334:254-9.

8. Safder S, Carpenter JS, Roberts TD, Bailey N. The "black turbinate" sign: An early MR imaging finding of nasal mucormycosis. AJNR Am J Neuroradiol 2010;31:771-4.

9. Joshi AR, Muthe MM, Patankar SH, Athawale A, Achhapalia Y. CT and MRI findings of invasive mucormycosis in the setting of COVID-19: Experience from a single center in India. Am J Roentgenol 2021;217:1431-32.

10. Taylor AM, Vasan K, Wong EH, Singh N, Smith M, Riffat F, *et al.* Black Turbinate sign: MRI finding in acute invasive fungal sinusitis. Otolaryngol Case Rep 2020;17:100222.

11. Manohar A, McCoy VA, Bazan C 3rd. Imaging features of invasive and noninvasive fungal sinusitis: A review. RadioGraphics 2007;27:1283-96.

12. Montone KT. Pathology of fungal rhinosinusitis: A review. Head Neck Pathol 2016;10:40-6.

13. Chakrabarti A, Denning DW, Ferguson BJ, Ponikau J, Buzina W, Kita H, *et al.* Fungal rhinosinusitis: A categorization and definitional schema addressing current controversies. Laryngoscope 2009;119:1809-18.

14. Gillespie MB, O'Malley BW Jr., Francis HW. An approach to fulminant invasive fungal rhinosinusitis in the immunocompromised host. Arch Otolaryngol Head Neck Surg 1998;124:520-6.

15. Yang X, Yu Y, Xu J, Shu H, Xia J, Liu H, *et al.* Clinical course and outcomes of critically ill patients with SARS-CoV-2 pneumonia in Wuhan, China: A single-centered, retrospective, observational study. Lancet Respir Med 2020;8:475-81.

16. Chen N, Zhou M, Dong X, Qu J, Gong F, Han Y, *et al.* Epidemiological and clinical characteristics of 99 cases of 2019 novel coronavirus pneumonia in Wuhan, China: A descriptive study. Lancet 2020;395:507-13.

17. Sen M, Honavar SG, Bansal R, Sengupta S, Rao R, Kim U. Epidemiology, clinical profile, management, and outcome of COVID-19-associated rhino-orbital-cerebral mucormycosis in 2826 patients in India-collaborative OPAI-IJO study on mucormycosis in COVID-19 (COSMIC), report 1. Indian J Ophthalmol 2021;69:1670-92.

18. El-Kholy NA, El-Fattah AM, Khafagy YW. Invasive fungal sinusitis in post COVID-19 patients: A new clinical entity. Laryngoscope 2021;131:2652-8.

19. Awal SS, Biswas SS, Awal SK. Rhino-orbital mucormycosis in COVID-19 patients-a new threat? Egypt J Radiol Nucl Med 2021;52:152.

20. Patil A, Mohanty HS, Kumar S, Nandikoor S, Meganathan P. Angioinvasive rhinocerebral mucormycosis with complete unilateral thrombosis of internal carotid artery-case report and review of literature. BJR Case Rep 2016;2:20150448.

21. Orlowski HL, McWilliams S, Mellnick VM, Bhalla S, Lubner MG, Pickhardt PJ, *et al.* Imaging spectrum of invasive fungal and fungal-like infections. Radiographics 2017;37:1119-34.

22. McLean FM, Ginsberg LE, Stanton CA. Perineural spread of rhinocerebral mucormycosis. AJNR Am J Neuroradiol 1996;17:114-6.

23. Galletta K, Alafaci C, D'Alcontres FS, Maria ME, Cavallaro M, Ricciardello G, *et al.* Imaging features of perineural and perivascular spread in rapidly progressive rhino-orbital-cerebral mucormycosis: A case report and brief review of the literature. Surg Neurol Int 2021;12:245.